

Highlights of Collaborated Research

Collaborative works with outside researches are carried out in consideration of the joint research program. Accepted applications are performed in following each division and facility of IMR.

1) Research Laboratories

Joint research conducted individually by outside researchers and IMR staff members at each research laboratory in the following view points: Originality, Fundamentality, Initiation and Promptness. Four categories "Research in Priority Area", "General Research", "Exploratory Research for Young Researchers" and "Workshop" are prepared. Outstanding achievements are posted in HP and in the present issue.



2) International Research Center for Nuclear Materials Science

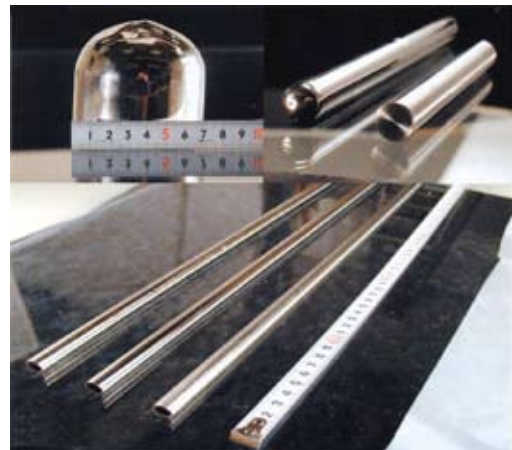
This facility is open to university scientists all over Japan to support experiments using Japan Materials Testing Reactor, JMTR, the fast experimental reactor, JOYO, and the test reactor, JRR-3, operated by JAEA (Japan Atomic Energy Agency). The overseas reactor, BR2, located at the Belgian Nuclear Research Center, is also used for irradiation experiments. This facility acts as a hub for international collaborations; specimens irradiated in overseas reactors are accepted here for post-irradiation examinations by participating university researchers. Research subjects covered here include fundamental studies and R&D on fusion structural materials, high heat-flux materials, and a variety of functional



materials, as well as engineering-oriented studies for the safety of light water reactors and basic researches supporting them. Materials studies utilizing radio-isotopes are also being conducted

3) Advanced Research Center of Metallic Glasses (ARCMG)

ARCMG was established in April 2006, succeeding the Laboratory for Advanced Materials (LAM), investigating metallic glasses and other materials. This facility is open to domestic and international collaborations for research on all aspects of materials science, consisting of two major divisions: (i) scientific research on fundamental properties of materials, and (ii) development of engineering materials for practical usage. Micromotors, pressure sensors, fuel cell separators, soft magnetic material and many other devices using metallic glasses are proposed for practical applications.



4) High Field Laboratory for Superconducting Materials

This laboratory restarted in 2001, succeeding "High Field Laboratory for Superconducting Materials" which was established in 1981. The main equipment is a hybrid magnet which generates steady high magnetic fields up to 31T. In addition, many cryogen-free superconducting magnets which have been developed by our laboratory are installed. Especially, we succeeded in developing the world's first cryogen-free hybrid magnet, which generates 27.5 T. The laboratory also provides instruments for measuring various physical properties. These facilities are open to scientists and engineers on superconductors

and other materials research.



5) Osaka Center for Industrial Materials research

The Osaka Center was established in Osaka as a special unit in IMR in April 2006 based on the agreement between Tohoku University and Osaka Prefecture Government. The mission is as following; solve the encountering technical problems in the enterprise, transfer academic findings to industries and provide education programs for the development of metallic materials. Research in the Osaka Center is focused on the understanding of the fundamentals of nano-structured metallic materials and the rapid realization of their application to industry, in particular, the small and medium enterprises in Osaka area.



6) Center for Computational Materials Science

This center was developed from the Laboratory of Materials Information Science which was established in February 1989. Its main tasks are 1) administration and maintenance of the supercomputing system in this Institute, 2) maintenance of a

supercomputing system network, 3) general support for the usage of the supercomputing system, 4) support of materials design by supercomputing simulation with vectorization and parallelization, 5) construction of factual database for materials, and 6) general support for the usage of Asian Consortium on Computational Materials Science - Virtual Organization.



7) International Collaboration Center (ICC-IMR)

ICC-IMR was founded after the International Frontier Center for Advanced Materials in April 2008. It has evolved into the international research collaboration center of Institute for Materials Research. As such, ICC-IMR's programs have been expanded to include collaborative research projects by international teams. It works as a gateway of diverse collaboration between international researchers and IMR members. Currently, ICC-IMR coordinates seven different programs: 1) International Integrated Project Research, 2) Visiting Professorships, 3) Short Single Research Visits, 4) Fellowship, 5) International Workshops and 6) Coordination of International Collaboration and 7) Material Transfer Program to foreign research institution for the international exchange. We welcome applicants from around the globe to participate in these international programs.



New Insight into Magnetic Interactions in Organic Radical Crystals

Magnetic properties of 2,3,6-trifluorophenyl nitronyl nitroxide have been examined in static and pulsed magnetic fields. The complementary analysis of the static susceptibility and high-field magnetization revealed the formation of two kinds of spin dimers each of which has a ground state of triplet ($S = 1$) and singlet ($S = 0$). Special molecular arrangements responsible for the magnetic interactions are extracted and the experimental evidence on the importance of the molecular overlap between the phenyl groups has been first observed.

One of the characteristic features in organic radicals is the softness and pentafluorophenyl nitronyl nitroxide has been reported to show the lattice distortion below 5 K, which suggests the presence of strong coupling between the phonon and magnetic exchange coupling. We have developed a series compound of fluorinated phenyl nitronyl nitroxides in order to reveal the magneto-structural correlations. The crystals of 2,3,6-trifluorophenyl nitronyl nitroxide show peculiar magnetic properties and new insight into the magnetic interactions were observed.

The temperature dependence of the product of the susceptibility and temperature ($\chi_p T$) takes a constant at two-thirds the room-temperature-value within 2 - 4 K. Magnetization (M) at 0.5 K is constant at half the value of full saturation within 2 - 5 T. The stationary values are seemingly curious but the complementary analysis of $\chi_p T$ and M has revealed the formation of two kinds of spin dimers with $S = 1$ and $S = 0$ in the ground state. This model well describes the $\chi_p T$ behavior and M in the low field region (Fig.1)

The full magnetization curve measured at 0.4 K is compared with the calculation in Fig.2. The gradual increase of magnetization above 10 T means the existence of the interdimer interactions.

The antiferromagnetic and ferromagnetic intermolecular interactions are assigned to the molecular arrangement shown in Fig.3(a) and

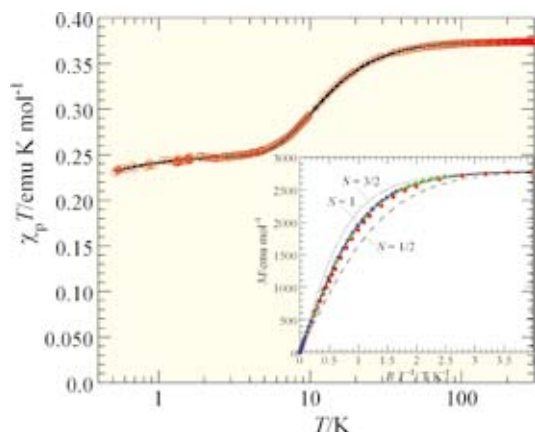


Fig. 1: Temperature dependence of $\chi_p T$. Inset: Magnetization curves below 5 T compared with Brillouin functions.

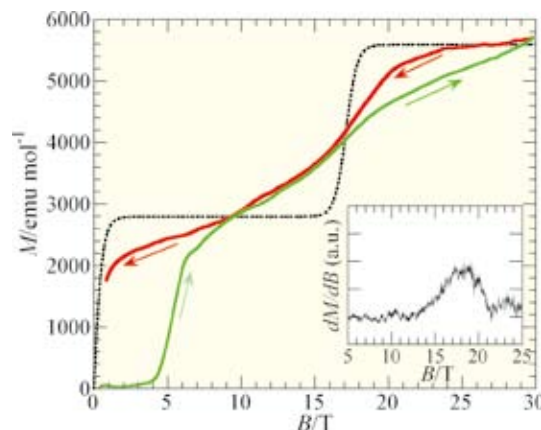


Fig. 2: Magnetization curve at 0.4 K in pulsed magnetic fields. Inset; dM/dB curve.

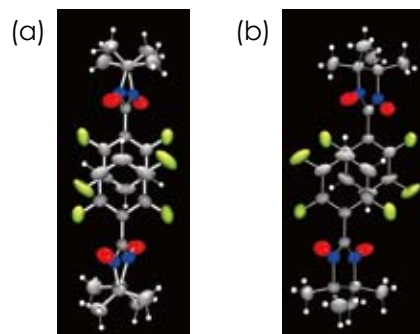


Fig. 3: Molecular arrangements responsible for (a) antiferromagnetic and (b) ferromagnetic interactions, respectively.

(b), respectively. This is the first evidence for the important role played by the relative arrangement of the phenyl groups among phenyl nitronyl nitroxide derivatives in the magnetic interactions.

References

- [1] T.Kanzawa, S.Nishihara, H.Nojiri and Y.Hosokoshi. Bull. Chem.Soc.Jpn., 83, 1447(2010).

Keywords: magnetic properties

Y.Hosokoshi¹ and H.Noiri²

1) Graduate School of Science, Department of physical science. Osaka Prefecture University,

2) IMR, Tohoku University,

E-mail: yhoso@p.s.osakafu-u.ac.jp

URL: <http://www.p.s.osakafu-u.ac.jp/~yhoso/index.html>

Appearance of Unique Strengthening Behavior of Dental Silver Alloy by Simple Heat Treatment

Dental silver alloy, Ag-20Pd-14.5Cu-12Au (mass%) exhibits unique hardening behavior after solution treatment. In this study, the effect of microstructure on the unique hardening behavior of this alloy was investigated. Results obtained from this study indicate that precipitated β' phase leads to this unique hardening behavior.

Ag-Pd-Au-Cu alloys are widely used in dental applications because they are cheaper than gold alloys, have good corrosion resistance, and exhibit good biocompatibility. Recently, it was reported that the mechanical strength of Ag-20Pd-12Au-14.5Cu (mass%) alloys subjected to solution treatment (ST) at temperatures over 1073 K followed by water quenching (WQ) without aging treatment was significantly enhanced. The origin of the unique hardening mechanism is not yet clear; only the relationship between the unique hardening behavior and the L1₀-type ordered β' phase precipitated in Ag-Pd-Au-Cu alloys has been reported [1]. However, studies of the formation processes or mechanisms of the L1₀-type ordered β' phase in as-solutionized Ag-Pd-Au-Cu alloys have been few in number. The purpose of this study is to investigate the effect of microstructure on the unique hardening behavior of Ag-Pd-Au-Cu alloy. In order to investigate, we compared with received materials (As-material) subjected to ST and the materials subjected to liquid rapid solidification (LRS) process and ST.

The microstructure of As-material is consisted of α_1 , α_2 and β phases. The microstructure of As-material changes to α , β , and β' phases through solution treatment (ST). The microstructure of LRS material is consisted of α , α_1 , and α_2 phases without β phase. The microstructure of LRS material through ST becomes single α phase. α_1 , α_2 and β phase are Cu-rich material, Ag-rich material and PdCu intermetallic compound, respectively.

Fig.1 shows bright field image obtained by TEM, diffraction pattern and key diagram of As-material subjected to ST for 3.6 ks. The coherent participation of β' phases with long and short axes of around 100 nm and 10 nm, respectively, also occurs during ST although the amount of β' phase decreases with increasing the ST time. The hardness and tensile strength of LRS material and LRS material subjected to ST are relatively smaller than those of As-material and As-material subjected to the ST. The Vickers hardness of As-materials with ST decreases with increasing the ST time longer than 3.6 ks. On the other hand, in the case of LRS materials, the Vickers hardness is not dependent on the ST time. In the case of As-materials with ST, the amount of precipitation

of metastable β' phase is influenced by ST time and it leads to precipitation strengthening[2].

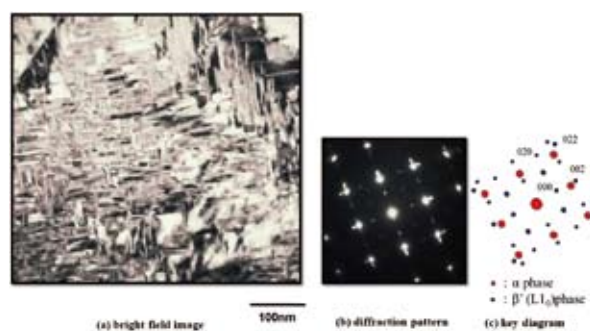


Fig. 1 TEM observation of As-material subjected to ST: (a) bright field image, (b) diffraction pattern and (c) key diagram. Beam direction is parallel to [100].

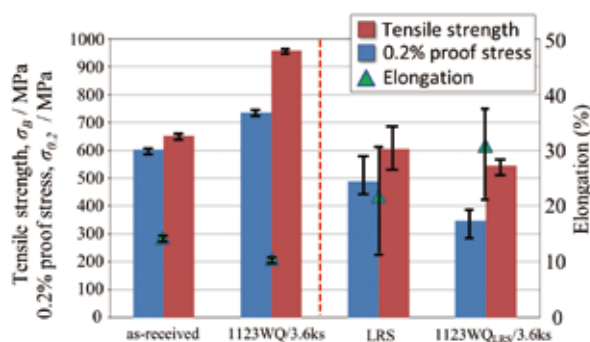


Fig.2 Tensile properties of As-materials and LRS materials subjected to ST.

References

- [1] Y. Tanaka, *Boundary* 19 (2003) 14–17.
- [2] T. Akahori, M. Niinomi, M. Nakai, H. Tsutsumi, T. Kanno, YH. Kim, H. Fukui, *J. Japan Inst. Metals*, 74 (2010) 6, 337–344.

Keywords: Biomedical, microstructure, strength
H. Fukui¹, M. Niinomi², M. Nakai²

1) School of Dentistry, Aichi-Gakuin University, 2) IMR, Tohoku University

E-mail: fukui@dpc.aichi-gakuin.ac.jp

High-purity Multicrystalline Silicon Production in a Unidirectional Solidification Furnace for Solar Cells

For accurate prediction of carbon and oxygen impurities in a single crystal produced by the Czochralski method, global simulation of coupled oxygen and carbon transport in the whole furnace was implemented. Both gas-phase transportation and liquid-phase transportation of oxygen and carbon were considered. With five chemical reactions considered, SiO and CO concentrations in gas and C and O atom concentrations in silicon melt were solved simultaneously.

Multicrystalline silicon has now become the main material in the photovoltaic market because of its low production cost and because of the relative high conversion efficiency of solar cells made from this material. The unidirectional solidification method is a cost-effective technique for large-scale production of multicrystalline silicon material. Similar to the Czochralski method, the unidirectional solidification is connected with transport of impurities [1]. Carbon and oxygen are two of the major impurities in multicrystalline silicon. If the carbon concentration exceeds 1×10^{16} atom/cm³, it will markedly influence the precipitation of oxygen during thermal annealing of crystals and during device processing of the wafers cut from these crystals [2].

The basic configurations of unidirectional solidification furnaces used in the study have been shown in the papers [3]. The graphite components in a furnace include heat shields, heaters and the crucible pedestal. They are the main sources of carbon elements in a grown crystal. The basic processes of carbon and oxygen incorporation into a crystal from the graphite components are shown in Fig. 1

Since most of carbon impurity in crystal is caused by the CO back-diffusion, we proposed to use a crucible cover to reduce the CO back-diffusion in the unidirectional solidification furnace [3]. The global simulation of coupled oxygen and carbon transports within the furnace was used to validate the feasibility of the improved design [3].

Numerical results shown in Fig.2 indicates that the oxygen concentration in the crystal can be reduced by at least 30% due to the increase of gas flow velocity near the melt surface if the crucible cover is placed. The detail can be referred to the paper [3].

References

- [1] H. Matsuo, R.B. Ganesh, S. Nakano, L.J. Liu, Y. Kangawa, K. Arafune, Y. Ohshita, M. Yamaguchi, K. Kakimoto, J. Cryst. Growth 310 (2008) 2204.
- [2] D.E. Borside, R.A. Brown, J. Electrochem. Soc. 142 (1995) 2790.
- [3] L.J. Liu, S. Nakano, K. Kakimoto, J. Cryst. Growth 303 (2007) 165.

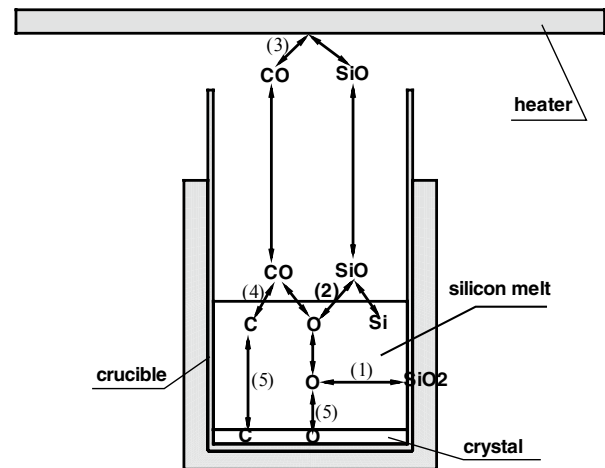


Fig. 1 Basic processes of carbon and oxygen incorporation into a crystal.

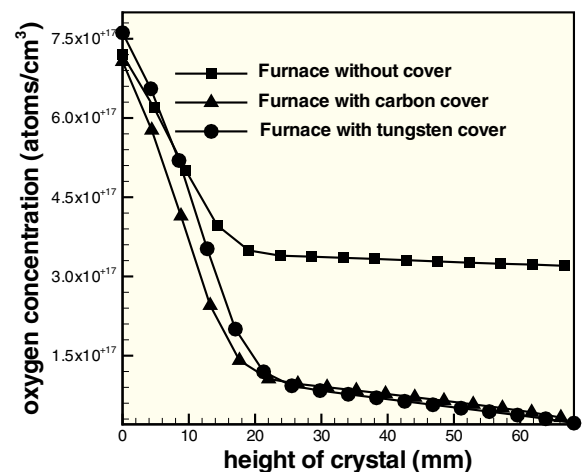


Fig. 2 Comparison of oxygen concentrations in the crystal for the old furnace and improved furnaces with different cover materials.

Keywords: simulation, solar cells
 K. Kakimoto B. Gao, S. Nakano,
 Research Institute for Applied Mechanics, Kyushu
 University, 6-1 Kasuga-koen, Kasuga, Fukuoka
 816-8580, Japan
 Tel) 81-92-583-7744
 E-mail: kakimoto@riam.kyushu-u.ac.jp
 URL: <http://www.riam.kyushu-u.ac.jp/taiharou/index.html>

Low energy magnetic excitations in the iron-based superconductor $\text{Fe}(\text{Se}_{1-x}\text{Te}_x)_y$

Magnetic fluctuations of $\text{Fe}_{1+x}\text{Se}_{0.45}\text{Te}_{0.55}$ ($x = 0, \delta$) are investigated by using neutron scattering technique. Non-superconducting $\text{Fe}_{1+\delta}\text{Se}_{0.45}\text{Te}_{0.55}$ shows a pronounced magnetic fluctuation around a reciprocal lattice 2D vector $\mathbf{Q}_{2D} = (0.5, 0)$. On the other hand, superconductor $\text{FeSe}_{0.45}\text{Te}_{0.55}$ shows a magnetic fluctuation at $\mathbf{Q}_{2D} = (0.5, 0)$ and $(0.5, \pm 0.5)$. This result suggests that the AF fluctuations characterized by $\mathbf{Q}_{2D} = (0.5, \pm 0.5)$ may play an important role in superconductivity.

The discovery of Fe-based superconductor has led to intensive studies on related superconductors including iron group. Their non-doped counterparts commonly exhibit an antiferromagnetic (AF) ordering, so that a precise understanding of the magnetic properties of the related compounds would provide a useful guideline for understanding the superconductivity. Therefore, the dynamical magnetic properties of the anti-ferromagnet (AF) $\text{Fe}_{1+\delta}\text{Se}_{0.45}\text{Te}_{0.55}$ ($T_N \approx 11$ K) and superconductor (SC) $\text{FeSe}_{0.45}\text{Te}_{0.55}$ ($T_c \approx 15$ K) have been investigated by inelastic neutron scattering techniques.

The measurements reported here show conclusively that a significant evolution occurs in the magnetic excitation spectra between AF and SC sample. Fig. 1 and 2 shows constant energy scans with the Gaussian fitting lines for AF and SC, respectively. For AF sample, the pronounced enhancement of the magnetic fluctuations at low energy ($E = 4$ meV) and significant decrease of intensity with increasing E were observed. The behavior confirms that this system is close to the AF ordered phase. On the other hand, for SC sample, a discernible scattering intensity peaks centered at $k = 0$ ($\mathbf{Q}_{2D} = (0.5, 0)$) and $k = \pm 0.5$ ($\mathbf{Q}_{2D} = (0.5, \pm 0.5)$) appear at $2 \text{ meV} < E < 6$ meV, and at $2 \text{ meV} < E < 10$ meV, respectively.

Qualitative difference between two samples is also observed from the peak position. Red lines of bottom of Figures show the peak centers of the magnetic excitation spectra for both samples at several temperatures. For AF sample, the magnetic excitations are located at $\mathbf{Q}_{2D} = (0.5, 0)$ at low energies ($E < 4$ meV). As E increases, the peak centers branch into substantially up to $(0.5, \pm 0.5)$ at $E \approx 10$ meV. For SC sample, the inelastic scattering intensities at $\mathbf{Q}_{2D} = (0.5, 0)$ decrease with increasing E , as is the case of AF sample. On the other hand, scattering intensities at $\mathbf{Q}_{2D} = (0.5, \pm 0.5)$ appears obviously, even above 6 meV. This suggests that the AF correlation with $\mathbf{Q}_{2D} = (0.5, \pm 0.5)$ may play an important role in the mechanism of superconductivity in Fe-based superconductors[1].

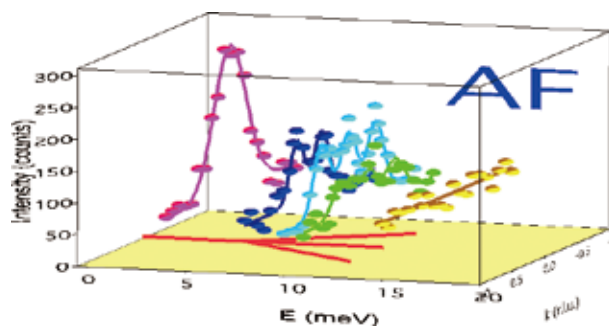


Fig. 1 Energy dependence of the inelastic scattering intensity for $\text{Fe}_{1+\delta}\text{Se}_{0.45}\text{Te}_{0.55}$ with $E = 4, 8, 10, 11$ and 15 meV at 10 K. Solid lines represent the results of fittings the data with a Gaussian line.

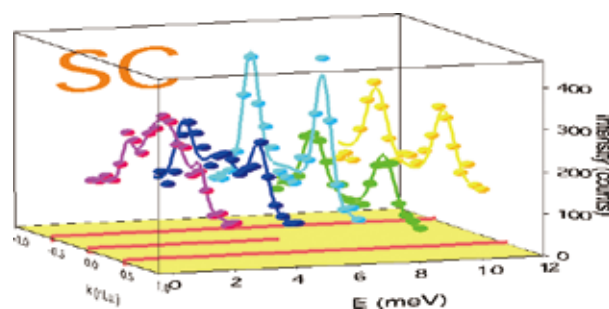


Fig. 2: Inelastic scattering intensity for $\text{FeSe}_{0.45}\text{Te}_{0.55}$ with $E = 2, 4, 6, 8$ and 10 meV at 10 K.

References

- [1] S. Iikubo, M. Fujita, S. Niitaka, H. Takagi, H. Ohtani, and M. Hasebe, *Physica C* 470, S401 (2010)

Keywords: neutron scattering, superconducting, magnetic properties
 S.Iikubo¹, M.Fujita², G.D.Gu³, and J.M.Tranquada³
 1) Kyushu Institute of Technology 2) IMR, Tohoku University 3) Brookhaven National Laboratory,
 E-mail:iikubo@life.kyutech.ac.jp

Computational Approach to Properties of Thermoelectric and Other Materials

Thermoelectric properties of clathrate compounds have been investigated by first-principles electronic structure calculations in order to explore the possibilities of high performance thermoelectric materials. Multi-scale simulations based on the molecular-dynamics/continuum hybrid method have been performed for polymer melt in order to demonstrate the usefulness of the present hybrid method.

We have studied thermoelectric properties of type-VIII $Ba_8Ga_{16}Sn_{30}$ (BGS) clathrates. BGS is an intrinsic semiconductor when the atomic composition is 8:16:30, being one of promising thermoelectric materials. Sn and Ga atoms compose the host cage structure and Ba atoms are encapsulated in the cages. The carrier type and the carrier concentration in BGS can be controlled by changing the atomic compositions of Sn and Ga. Ga atoms are distributed at random in the host framework.

In the previous work [1], we calculated the electronic structures and thermoelectric properties of BGS with the Ga configuration determined by experimental results. In the present study we have calculated the electronic structures of BGS with different Ga configurations to discuss the effect of Ga distribution on thermoelectric properties.

We have performed first-principles electronic structure calculations of type-VIII BGS using the super-cell approximation, and then calculated the thermoelectric power (TEP) using the calculated electronic structures. The temperature dependences of TEP for different Ga configurations are shown in Fig. 1.

We have developed a computational method coupling atomic model and macro-scale continuum [2], and applied the method to polymer melt consisting of long chain polymers. The polymer molecule is coarse-grained into a meso-scopic model by the so-called spring-beads model. This spring-beads model is coupled with an elastic continuum using our hybrid method.

Fig. 2 shows the usefulness of multi-scale simulations based on our hybrid method. The simulation time required to achieve the equilibrium state is reduced drastically compared with conventional equilibration methods. The polymers can move with a wide range of energy due to large scale fluctuations generated by the elastic continuum, and a variety of chain structures are generated in the polymer melt. This situation results in the fast convergence to the equilibrium state of long chain polymers.

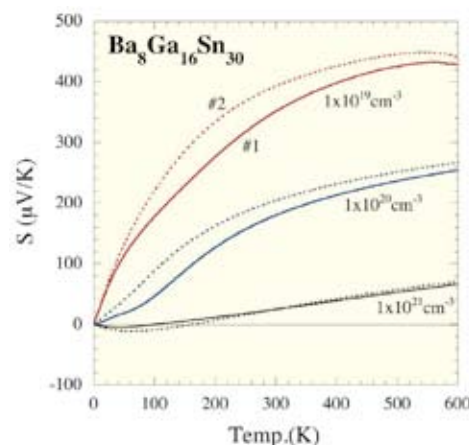


Fig. 1: Calculated thermoelectric power of BGS with n-type carriers.

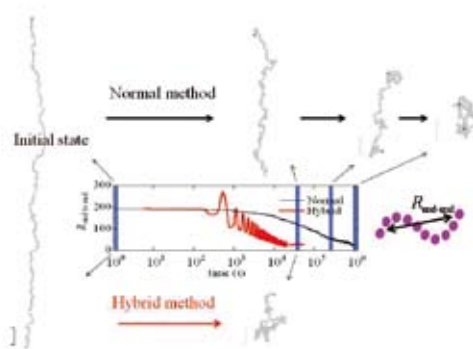


Fig. 2: Time evolution of the end-end distance of polymers and chain structures of a polymer.

References

- [1] Y. Kono, N. Ohyama, T. Taguchi, K. Suekuni, T. Takabatake, S. Yamamoto, and K. Akai: J. Appl. Phys., 107, 123720/1-6 (2010).
- [2] Y. Senda and G. Kim, Prog. Theor. Phys. Suppl. Vol. 178, 141 (2009).

Keywords: ab initio calculation, thermoelectric, simulation

K. Akai¹, Y. Senda², and S. Shimamura²

1) Media and Information Technology Center, Yamaguchi University

2) Faculty of Engineering, Yamaguchi University

E-mail: akai@yamaguchi-u.ac.jp

senda@yamaguchi-u.ac.jp

simamura@yamaguchi-u.ac.jp

Plasma Purification of Ag Nanoparticles to Control Localized Surface Plasmon Resonance

Remarkable changes, blueshift and narrowing, in localized surface plasmon resonance of silver NPs without significant morphological modifications have been demonstrated with plasma treatments. Our findings provide information on the reason why most of the experimental extinction spectra of the NPs on substrates are considerably different from those generated by simulation based on Mie's theory.

The control of the surface plasmon resonance property, which is well characterized by the plasmon resonance wavelength λ_p and line width $\Delta\omega_p$, is required for silver nanoparticles (NPs) supported on substrates to realize applications of chemical and biological sensors. In the survey of the λ_p of supported silver NPs, it is found that the reported λ_p values are between 380 and 500 nm, larger than that predicted by the Mie's theory (370 nm); the experimental data vary from lab to lab. Further, most of the optical extinction spectra reported are found to be much broader than the calculated one. The shape and density (or degree of dispersion) of silver NPs on substrates are, of course, factors to govern their optical properties, but the variation of the reported λ_p as well as the discrepancy between experimental and theoretical extinction spectra cannot be explained completely by these two factors. To control the surface plasmon properties, all the occurring effects should be clarified.

We have demonstrated that plasma purification of silver NPs brings about blueshift and narrowing in their localized surface plasmon resonance, as has been shown in Fig. 1 [1]. To confirm the origin of the changes in the surface plasmon property, Raman scattering, scanning electron microscopy, Rutherford backscattering spectrometry were conducted.

Extremely high sensitivity for adsorbed molecules on silver NPs can be expected due to surface enhanced Raman scattering (SERS). The SERS analysis revealed that hydrocarbons adsorbed on silver surfaces were removed effectively by plasma exposure. As can be seen in Fig. 2, the decrease in Raman intensity for hydro-carbons is correlated well with the blueshift.

Our findings indicate that one of the most important factor for remarkable differences in plasmon resonance wavelengths and line widths reported for the silver NPs supported on substrates between most of the experimental data and calculations based on Mie's theory is due to the impurity adsorption on silver surfaces. Plasma purification would enable us to control the optical properties of other metallic NPs.

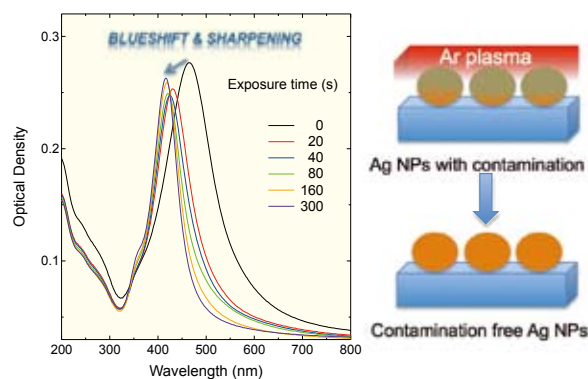


Fig. 1: Optical extinction spectra of Ag NPs deposited onto SiO₂ before and after plasma treatments (left), together with a schematic drawing of Ar plasma purification (right).

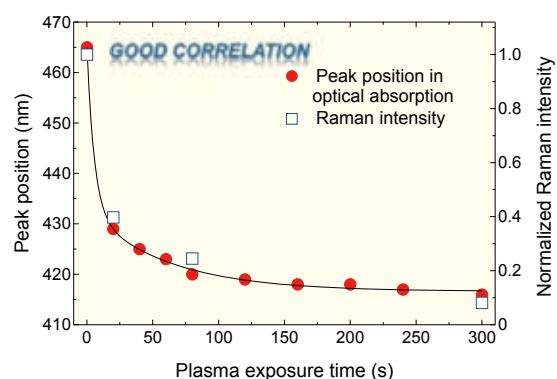


Fig. 2: Peak positions of surface plasmon resonance band in the extinction spectra (filled circles) and normalized Raman intensities (open squares) as a function of plasma exposure time. A line is drawn to guide the eyes.

References

- [1] K. Kawaguchi, M. Saito, K. Takahiro, S. Yamamoto, M. Yoshikawa, *Plasmonics*, 6, 535 (2011).

Keywords: nanoparticle, optical absorption

K. Takahiro¹ and S. Nagata²

1) Graduate School of Science and Technology, Department of Chemistry and Materials Technology, Kyoto Institute of Technology, 2) IMR, Tohoku University.

E-mail: takahiro@kit.ac.jp

Development of Rapid Surface-Nitriding System Using a Microwave-Induced Nitrogen Plasma at Atmospheric Pressure

Rapid surface-nitriding system for surface modification of steels has been developed by using an apparatus equipped with a microwave-induced nitrogen-plasma generator. The new system can produce the nitrided layer having a thickness of several micrometer within one minute, which is 10^{-2} times of the conventional surface-nitriding techniques.

Nitriding treatment has been extensively used for surface modifications of steels. Nitrogen radicals such as excited nitrogen molecules and nitrogen molecule ions act as reactants in the plasma nitriding process. The conventional plasma-nitriding techniques, which are conducted under evacuated atmospheres, require several hours for obtaining nitrided layers having several-micrometer thickness. According to our studies, the population of the nitrogen radicals affects the surface-nitriding reaction [1], suggesting that the slow nitriding reaction of the conventional techniques can be ascribed to the low population of the nitrogen radicals. Therefore, to achieve the rapid nitriding treatment, we developed a new plasma-nitriding apparatus, which can produce high-population nitrogen radicals by the plasma in atmospheric pressure.

Fig. 1 shows the setup of the newly developed apparatus. The apparatus comprises a microwave generator, a waveguide, an Okamoto cavity [2] and torch. The microwave power is transmitted to the Okamoto cavity through the waveguide. N_2 gas was introduced into the torch at atmospheric pressure, and a flame-like N_2 plasma was formed above the torch. In this study, an iron plate was used for a specimen, which was located near the apex of the plasma. The microwave power was fixed at 700 W to heat the sample at a moderate temperature between 700 and 800 K.

Fig. 2 shows a depth profile of elements for the nitrided iron surface [3]. The nitriding-treatment time was 40 s. Whereas conventional plasma-nitriding techniques would require several hours for nitriding treatments, this result demonstrates that the newly developed system is able to produce a nitrided layer having a thickness of several micrometer within one minute. The nitrided layer is composed of two layers containing different nitrogen concentration of about 20% and 10%. According to the X-ray diffraction pattern of the specimen, the 20%-nitrogen and 10%-nitrogen layers consist of Fe_4N and γ -Fe, respectively. It should be noted that the nitrogen concentration of γ -Fe layer almost reaches the solubility limit of nitrogen in γ -Fe, suggesting that the nitrogen reactant is supplied at a high rate into the specimen surface by the radical-rich plasma. This phenomenon also exhibits a peculiar feature of the nitrided layer formed with the new system.

It is expected that the present surface-nitriding system is applicable to the surface treatment of various base metals such as aluminum and titanium. The application to these materials is in progress now.

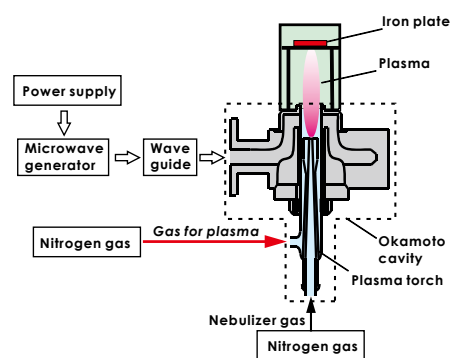


Fig. 1 Schematic diagram of the setup of the rapid surface-nitriding system using a microwave-induced nitrogen plasma.

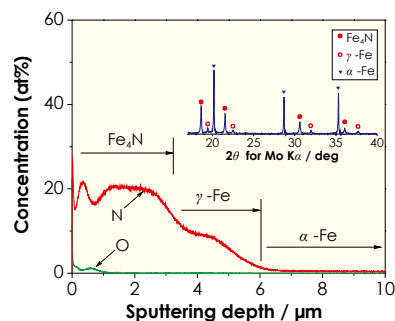


Fig. 2 Depth distribution of elements of the iron plate nitrided by the newly developed apparatus. The inset shows the X-ray diffraction pattern of the nitrided specimen.

References

- [1] S. Sato, K. Omori, S. Araki, Y. Takahashi, K. Wagatsuma, *Surf. Interface Anal.*, **41**, 496 (2009).
- [2] Y. Okamoto, *Anal. Sci.*, **7**, 283 (1991).
- [3] Y. Arai, S. Sato, N. Yamashita, A. Kojo, Y. Okamoto, K. Wagatsuma, *CAMP-ISIJ*, **23**, 478 (2010).

Keywords: nitride, surface reaction
 Y. Okamoto* (Toyo University)
 S. Sato and K. Wagatsuma (Tohoku University)
 * Faculty of Science and Engineering, Toyo University
 E-mail: okamoto@toyo.jp

Microscopic Evidence for the 8.5 K Phase Transition in Americium Dioxide Proved by NMR

More than 30 years ago, a phase transition was suggested to occur in americium dioxide at 8.5 K based on magnetic susceptibility data, while no evidence had been obtained from microscopic measurements. Owing to the limited number of experiments, the mechanism of this phase transition has remained a mystery. Recently ^{17}O NMR provides the first microscopic evidence for a phase transition as a bulk property in this system.

A phase transition in americium dioxide (AmO_2) was first reported in 1975 from magnetic susceptibility data, which showed a broad maximum around $T_0=8.5$ K [1]. This behavior has been attributed to an ordinary magnetic dipolar ordering similar to that of UO_2 . However, this interpretation was not consistent with two other experimental results reported around that time: ^{243}Am Mössbauer spectroscopy and neutron diffraction measurements indicated the absence of ordered dipolar moments at the Am sites below T_0 . Up to now, except for the susceptibility data, there has been no experimental result to support the occurrence of a bulk phase transition in AmO_2 .

In this study, we have prepared a powder sample of $^{243}\text{AmO}_2$ containing 90 at. % ^{17}O and have performed ^{17}O NMR [2]. The phase transition has been detected as a sudden loss of NMR signal intensity below T_0 . With further decrease of temperature, the NMR signal reappears and a spectrum with extreme broadening has been observed. The observed spectrum covers a range of ~ 14 kOe in applied field, as shown in Fig.1. These data provide the first microscopic evidence for a phase transition as a bulk property in this system. Interestingly, the spectrum has been found to split into two peaks even in the paramagnetic state, an effect which has not been reported for actinide dioxides studied up to now. We suggest that the splitting is induced by self-radiation damage from the alpha decay of ^{243}Am .

In localized f -electron systems, the electron state is represented in terms of multipole degrees of freedom. For AmO_2 , the Am^{4+} crystalline electric field (CEF) ground state was believed to be the Γ_7 doublet, which carries only dipole degrees of freedom. Recently, however, Hotta has pointed out that the ground state could be a Γ_8 quartet for the same CEF potential [3]. For such a case, multipolar ordering is expected, since the Γ_8 quartet carries quadrupolar and octupolar degrees of freedom.

The present NMR also tells us that to avoid complexities arising from sample aging, data from a very fresh sample are essential for the study of AmO_2 . In this context, we suggest that the past results for Mössbauer spectroscopy and neutron diffraction need to be reexamined

with careful attention paid to effects of sample aging. To determine the order parameter of AmO_2 , the NMR in a fresh sample is now in preparation.

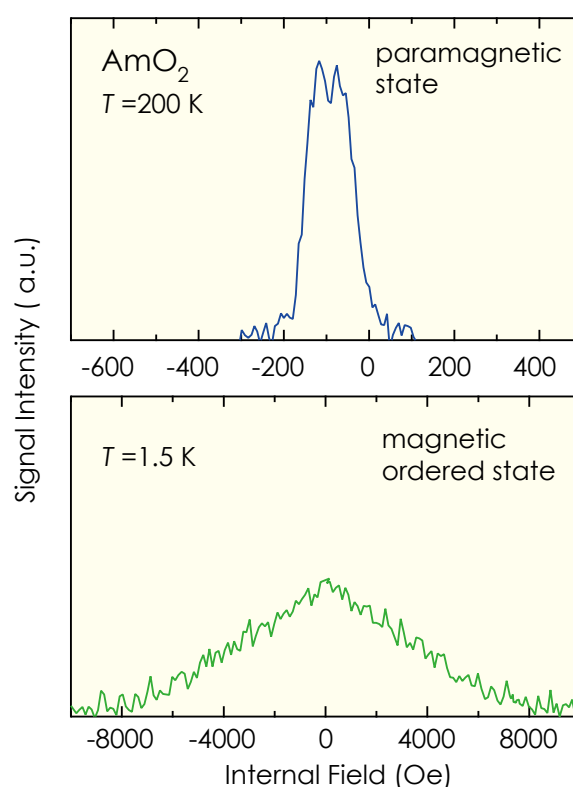


Fig. 1 Temperature dependence of ^{17}O NMR spectrum in AmO_2 .

References

- [1] D.G.Karraker, J. Chem. Phys. **63**, 3174 (1975).
- [2] Y.Tokunaga, T.Nishi, S.Kambe, M.Nakada, A.Itoh, Y. Homma, H.Sakai, and H.Chudo, J. Phys. Soc. Jpn. **79**, 053705 (2010).
- [3] T.Hotta, Phys. Rev. **B 80**, 024408 (2009).

Keywords: actinide, magnetic properties, nuclear magnetic resonance (nmr)

Yo Tokunaga¹ and Yoshiya Homma²

1) ASRC, Japan Atomic Energy Agency, 2) IMR, Tohoku University

E-mail: tokunaga.yo@jaea.go.jp

URL: <http://asrc.jaea.go.jp/soshiki/gr/kambe-gr/EnglishSites/>

New Kind of Volcano on the Earth —Geochronological Studies of Neutron-Irradiated Lavas Erupted on the Sea Floor—

Tectonic plate boundaries are marked by volcanoes, earthquakes, and related geologic activity; however, a new kind of volcano, named “petit-spot”, has recently been found in regions located far from plate boundaries. Newly discovered lavas produced by petit-spot volcanoes have been dated using the Ar–Ar technique.

Rigid tectonic plates move around the surface of the Earth on top of the asthenosphere (ductile part of the mantle), which marks the upper limit of convection in the mantle. Hirano et al. [1] reported the discovery of young volcanoes located far from tectonic plate boundaries (e.g., mid-oceanic ridges and volcanic arcs), which are the usual sites of volcanoes, earthquakes, and related geologic activity. The newly found volcanoes, named “petit-spot”, occur in a region of the Pacific Plate that is susceptible to fracturing prior to plate subduction at the Japan Trench off NE Japan. The magmas originate from the asthenosphere immediately under the plate.

Radiometric Ar–Ar dating is commonly used to determine the ages of deep-sea lavas. Samples for dating were irradiated by neutrons in a reactor (JMTR or JRR3) to produce ^{39}Ar from ^{39}K . Then, radiogenic ^{40}Ar , daughter nuclide of radioactive ^{40}K and parent (^{39}Ar instead of ^{40}K) were simultaneously analyzed using a multi-step heating technique and mass spectrometer [2]. This method is employed to distinguish radiogenic ^{40}Ar from inherited one from the mantle, which inhibits the dating of lava especially erupted in deep sea.

Ar–Ar dating of four petit-spot volcanoes indicates that the magmas were erupted from 1.8 to 8.5 million years ago [1–3]. Much younger date (an age between 0.05 and 1 million years ago) was obtained afterward for another petit-spot [1]. These ages are surprisingly young, because nearby seamounts and the Pacific Plate were formed at around 100 million years ago.

Other geophysical and geochemical evidence indicates that lavas from petit-spot volcanoes derive from partially melted rock from the asthenosphere, where melt forms and accumulates due to concave flexing of the plate as it approaches the subduction zone [4]; the magma is squeezed through cracks in the overlying tectonic plate (Fig. 1). This model would indicate that such volcanoes are ubiquitous on the ocean floor, where incipient melts are squeezed upward through fractures by tectonic forces associated with plate flexure [3]. Several research cruises have found petit-spot volcanoes in other areas of the Pacific (e.g. off the Chile Trench [5]).

The physical state and geochemical

characteristics of the asthenosphere remain largely unknown, despite its importance in terms of plate tectonics. Further studies of petit-spot lavas will provide important information on the asthenosphere and the nature of tectonic plates [6–8].

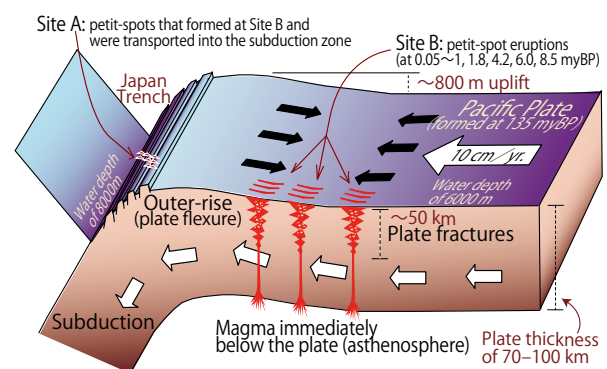


Fig. 1: Schematic model of the petit-spot volcanoes generation [1]. myBP = million years before present. White arrows show the motion of the Pacific Plate, which moves at 10 cm per year. Petit-spots erupt along the fractures that develop in response to this surface stress due to plate flexure (black arrows).

References

- [1] N.Hirano, E.Takahashi, J.Yamamoto, N.Abe, S.P.Ingle, I. Kaneoka, J.Kimura, T.Hirata, T.Ishii, Y.Ogawa, S.Machida and K.Suyehiro. *Science*, **313**, 1426 (2006).
- [2] N.Ebisawa, H.Sumino, R.Okazaki, Y.Takigami, N.Hirano, K.Nagao and I.Kaneoka. *J. Mass Spectr. Soc. Japan*, **52**, 219 (2004).
- [3] N.Hirano, A.A.P.Koppers, A.Takahashi, T.Fujiwara and M.Nakanishi. *Basin Res.*, **20**, 543 (2008).
- [4] G.Valentine and N.Hirano. *Geology*, **38**, 55–58 (2010)
- [5] N.Hirano. *EOS Trans. AGU.*, **91**, V13F-07 (2010)
- [6] N.Hirano. *Geochem. J.*, **45**, 157 (2011).
- [7] S.Machida, N.Hirano and J.Kimura. *Geochim. Cosmochim. Acta*, **73**, 3028 (2009).
- [8] J.Yamamoto, N.Hirano, N.Abe and T.Hanyu. *Chem. Geol.*, **268**, 313 (2009).

Keywords: geologic, mass spectroscopy, neutron irradiation

Naoto Hirano

(Center for NE-Asian Studies, Tohoku University)

E-mail: nhirano@m.tohoku.ac.jp

URL: <http://www.f2.dion.ne.jp/~nhirano/>

Co-Doping of Mn and V to LaNbO₄ for Ferromagnetic-Ferroelastic Novel Material

For realization of ferromagnetic-ferroelastic novel material, Mn and V were co-doped to LaNbO₄. Ferromagnetic transition occurred at ≈ 200 K for the LaNb_{0.6}V_{0.1}Mn_{0.3}O₄ sample having monoclinic crystal structure. Glassy behavior reflects exchange interaction between Mn⁴⁺(d³)NbO₇ clusters via Vo[•]. Formation of magnetic nanoclusters by acceptor doping is advantageous for development of stress-switchable information storage material.

LaNbO₄ has two polymorphs: the scheelite structure with tetragonal symmetry (*t*-LaNbO₄; *I*4₁/a) and the fergusonite structure with monoclinic symmetry (*m*-LaNbO₄; *I*2/c). Below 770 K, *t*-LaNbO₄ transforms into more stable *m*-LaNbO₄. Ferroelasticity of *m*-LaNbO₄ is advantageous to develop non-volatile information storage material controllable with nanoscale stress by piezoresponse force microprobe.

For extension of functionality of *m*-LaNbO₄ to ferromagnetism (FM) in nanoscale, we substituted Nb⁵⁺ by Mn⁴⁺ and V⁵⁺ [1]. Both increasing the dopant content and introduction of oxygen vacancy (Vo) are important for realizing FM in nanoscale. The solution energy with doping depends on ionic radii (*r*_{ion}). Although *r*_{ion} of V⁵⁺ (0.036 nm) is smaller than that of Nb⁵⁺ (0.048 nm), V⁵⁺ substitutes for Nb⁵⁺ and forms *t*-LaNb_{0.7}V_{0.3}O₄ crystal (Fig. 1 upper left). Since *r*_{ion} of Mn⁴⁺ (0.039 nm) is similar to that of V⁵⁺, substitution of Mn⁴⁺ for V⁵⁺ is expected to show the lowest solution energy, and generate Vo to maintain electrical neutrality.

Powders of La₂O₃, Nb₂O₅, V₂O₃, and Mn₂O₃ weighed with the molar ratio of [La] : [Nb] : [V] : [Mn] = 1 : 0.6 : 0.1 : 0.3 were mixed in grinding, and then heated at 1573 K in flowing oxygen gas for 4 h. The sample with nominal composition of LaNb_{0.6}V_{0.1}Mn_{0.3}O₄ demonstrated X-ray diffraction pattern (Fig.1 upper right) of isomorphous with *m*-LaNbO₄. As seen in Fig. 1 middle panels, the sample exhibited FM behavior in temperature- and field-dependences of magnetization (M-T & M-H). The (1/M)-T curve indicated the Curie temperature of ≈ 200 K. A small coercive field of the sigmoidal M-H curve suggests that the FM behavior is originated from magnetic nanoclusters. Frequency dependence of the in-phase ac-magnetization (M') showed glassy behavior (Fig.1 lower left) based on exchange interaction between the nanoclusters.

The tetrahedron, where Mn⁴⁺ substituted for V⁵⁺, loses oxygen, and reconstruction occurs to form MnNbO₇ linking cluster sharing a corner-oxygen (Fig. 1 lower right). Thus, exchange interaction between Mn⁴⁺(d³)NbO₇ clusters via singly ionized Vo[•] results in effective M of $\approx 2\mu_B/\text{Mn}$ for the nominal composition.

Our research on LaNb_{0.6}V_{0.1}Mn_{0.3}O₄ is a

challenge of material development toward stress-switchable nanoscale memory.

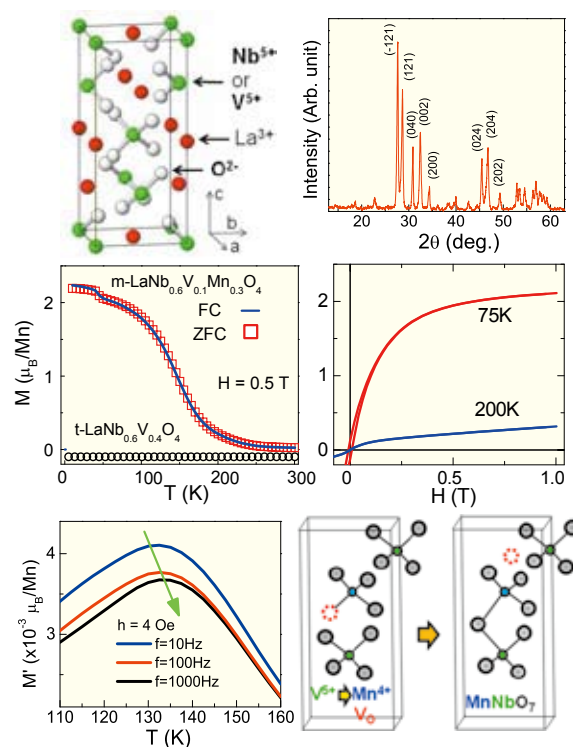


Fig.1 Schematic representation of *t*-LaNb_{0.7}V_{0.3}O₄ crystal structure (upper left), X-ray diffraction pattern of the LaNb_{0.6}V_{0.1}Mn_{0.3}O₄ sample (upper right), M-T (middle left) of the sample with that of LaNb_{0.6}V_{0.4}O₄ as a reference (ZFC), M-H (middle right) and M'-T at various frequency (lower left) of the sample, and schematic representation of MnNbO₇ cluster formation with Vo (lower right).

References

- [1] K.Okada, S.Kawakami, S.Kohiki, H.Shimooka, H.Deguchi, M.Mito, T.Shishido and M.Mitome: Ext. Abst. 71st Autumn Meeting, 2010; Jpn. Soc. Appl. Phys. 16a-NH-4.

Keywords: ferromagnetic, nanocluster, defects S.Kohiki¹ and K.Yubuta²

1) Department of Materials Science, Kyushu Institute of Technology, 2) IMR, Tohoku University
E-mail: kohiki@che.kyutech.ac.jp
URL: <http://www.che.kyutech.ac.jp/chem13/chem13.htm>

Development of Diamond Photonic Crystals Composed of Metallic and Oxide Glasses Lattices for Terahertz Waves Control

Photonic crystals with periodic arrangements of magnetic permeability and dielectric constant were fabricated to diffract and control electromagnetic wave propagations in terahertz frequency ranges. Metallic glass particles of $\text{Fe}_{72}\text{B}_{14.4}\text{Si}_{9.6}\text{Nb}_4$ composite were dispersed into micro oxide glass lattices of $\text{B}_2\text{O}_3 \cdot \text{Bi}_2\text{O}_3$. The photonic crystals with diamond structures were created by using micro patterning stereolithography and powder sintering process.

Photonic crystals with periodic vibrations in magnetic permeability or dielectric constant exhibit forbidden gaps in electromagnetic waves transmission spectra by Bragg diffraction. Introduced air cavities of structural defects can resonate and localize the electromagnetic waves with specific wavelengths and form localized modes of transmission peaks in the photonic band gaps. By applying original micro patterning stereolithography and powder sintering process [1,2], the photonic crystals with a diamond structure composed of minute oxide glass lattices of $\text{B}_2\text{O}_3 \cdot \text{Bi}_2\text{O}_3$ including metallic glass particles of $\text{Fe}_{72}\text{B}_{14.4}\text{Si}_{9.6}\text{Nb}_4$ were fabricated successfully as shown in Fig. 1. The iron based metallic glass is soft magnetic amorphous alloys with the high glass forming ability and high magnetic permeability. Geometric patterns of the dielectric or magnetic micro lattices were modified and optimized to control the electromagnetic waves belonging to terahertz frequency ranges effectively by using computer aided design, manufacture and evaluation. The terahertz waves can be synchronized with collective vibration modes of various organic matters and biological microbes. The formed photonic crystals are expected to be applied for environmental sensors to detect harmful substances and bacteria seedbeds for observation of the living behaviors through terahertz wave time domain spectroscopy. To create the micro lattices, the metallic and oxide glasses particles of 5 μm in average diameter at 17 and 23 vol. % were dispersed into photo sensitive acrylic resins, respectively. The resin paste was spread on a substrate with 10 μm in layer thickness by using a mechanical knife edge, and cross sectional images of an ultra violet ray were exposed by a digital micro mirror device with 2 μm in part accuracy. After the layer stacking, the obtained precursors were heated at 490 $^\circ\text{C}$ for 0.5 hs in vacuum for the dewaxing and sintering. This heating temperature is above the melting point of the oxide glass and under the crystallization point of the metallic glass. Fig. 2 shows a microstructure of the oxide glass lattice including the metallic glass particles. In the X-ray analysis, diffraction profiles indicating amorphous structures were observed.

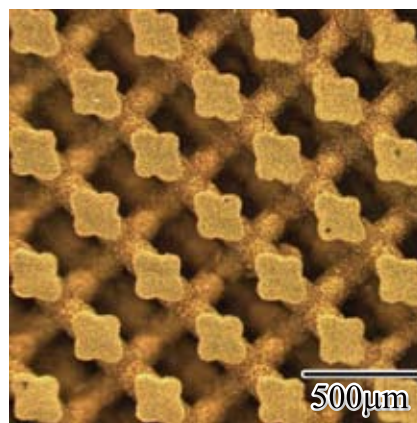


Fig.1 A diamond photonic crystal composed of magnetic and dielectric lattices formed by micro patterning stereolithography and powder sintering process.

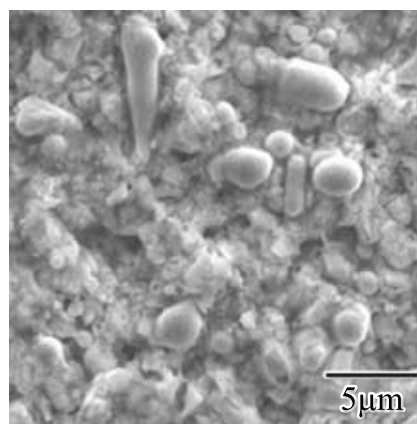


Fig.2 A microstructure in oxide glass lattice of $\text{B}_2\text{O}_3 \cdot \text{Bi}_2\text{O}_3$ including metallic glass particles of $\text{Fe}_{72}\text{B}_{14.4}\text{Si}_{9.6}\text{Nb}_4$ observed by using a scanning electron microscopy.

References

- [1] S.Kirihara, N.Komori and N.Ohta, *Advances in Science and Technology*, 63, 141 (2010).
- [2] S.Kirihara, T.Niki and M.Kaneko, *Ceramic Transactions*, 126, 113 (2010).

Keywords: photonic crystals, metallic Glass
 S.Kirihara¹ and H. Kato²
 1) JWRI, Osaka Univ., 2) IMR, Tohoku Univ.
 E-mail: kirihara@jwri.osaka-u.ac.jp
 URL: <http://www.jwri.osaka-u.ac.jp/~mri1>

Hydrogen Production from Methanol Steam Reforming over Catalysts Prepared from Cu-Zr Amorphous Alloys

Amorphous metallic alloys, Cu-Zr, have been studied as catalyst precursors for methanol steam reforming to produce hydrogen. The addition of a very small amount of noble metals enhanced the activity without an increase in carbon monoxide formation. Recently, the activity was increased by a factor of 100 by improving the conditions of pretreatment.

Methanol steam reforming is one of promising method to produce hydrogen for small-size fuel-cell units. It is reported that catalysts prepared from Cu-Zr amorphous alloys had the activity for this reaction when a small amount of noble metals such as platinum and rhodium were contained [1]. Carbon monoxide is a poison for the electrodes of fuel cells and is formed over Pt catalysts. However, by controlling the noble metal content, the formation of carbon monoxide was successfully suppressed.

The amorphous alloy ribbons were prepared at the IMR, Tohoku University, by single-roll rapid solidification. The alloy was cut, calcined in the air and reduced by hydrogen in the previous study. After these treatments, the reaction was performed and was followed by regeneration involving calcination and reduction. The activity reached a maximum after several repetitions of the regeneration and reaction.

We have studied the pretreatment method and condition [2]. The experiments provided that the activity was drastically increased by suitable pretreatment. In the improved method, after the hydrogen reduction, the alloy was ground and used for the reaction test.

Fig.1 shows the comparison between the conversions by the previous pretreatment and by the improved method. The methanol conversion, x_A , was converted a function using a logarithmic function; $-\ln(1-x_A)$ to indicate the activity linearly. The horizontal axis is the reverse of temperature. The apparent activation energy was estimated from the slope of the line in this figure to be 73.2 kJ/mol.

The activity of the catalysts prepared by the improved pretreatment shows an increase of 2 orders of magnitude. The temperature to obtain the same activity was decreased by about 100 K for the improved catalyst.

The optimum Pt content to obtain the high activity had both the lower and upper limits. When the alloy, Cu₅₀Zr₅₀ was used, the optimum Pt content was between 0.1 and 0.2 at% as shown in Fig.2.

When the previous method was applied, the activity gradually decreased with process time. The activity was stable after an initial decrease for the improved method. However, the selectivity for carbon monoxide was still

above 100 ppm and it is required to improve this point.

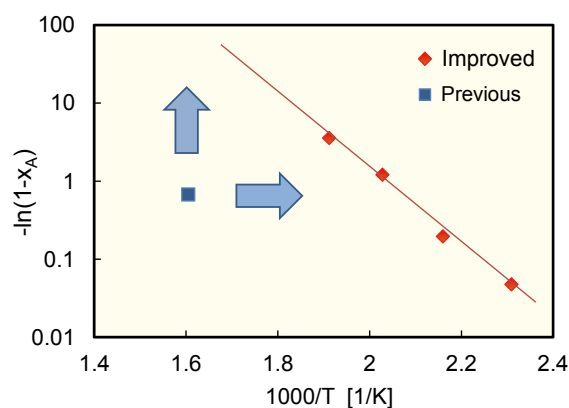


Fig. 1: Increase in the catalytic activity by improving pretreatment method.

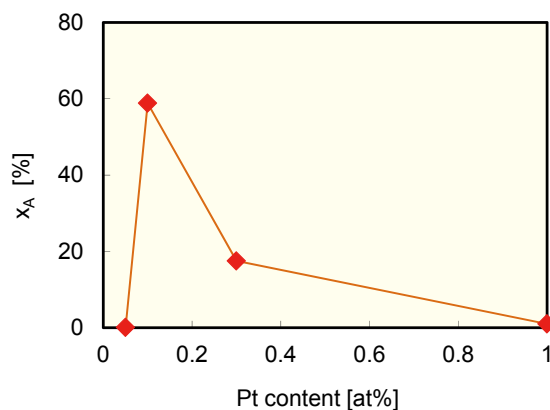


Fig. 2: Effect of platinum content on the catalytic activity.

References

- [1] T.Takahashi, M.Kawabata, T.Kai, H.Kimura and A. Inoue, J. Japan Inst. Metals., 71, 615 (2007).
- [2] A.Hirata, T.Kai, T.Nakazato, H.Kimura and T.Goto, Proc. of 23rd Int. Symp. on Chem. Eng., PF-03, Fukuoka, Japan (2010).

Keywords: alloy, amorphous, catalytic
T.Kai¹ and H.Kimura²

1) Department of Chemical Engineering, Graduate School of Science and Engineering, University of Kagoshima, 2) IMR, Tohoku University
E-mail:t.kai@cen.kagoshima-u.ac.jp

Observation of Fractional Quantum Hall Effect at $\nu = 1/3$ in a MgZnO/ZnO Heterointerface under High Magnetic Field

The Fractional quantum Hall effect (FQHE) is one of the most prominent quantum phenomena and has been observed in extremely high-mobility electron and hole two-dimensional systems at low temperature under high magnetic field. Owing to the improved quality of the MgZnO/ZnO heterointerface, we observed FQHE at $\nu = 1/3$ for the first time in oxide systems.

The MgZnO/ZnO (Mg = 1 %) heterostructure was grown by molecular beam epitaxy on Zn-polar ZnO (0001) substrate. In this structure, high-mobility two-dimensional electron gas (2DEG) is formed at the interface by the polarization discontinuity between MgZnO and ZnO as schematically shown in the inset of Fig. 1 [1]. Unique to our growth system, pure ozone was employed as an oxygen source, by which the impurity concentration incorporated to the film can be considerably reduced. As a result, the mobility of the 2DEG reached $300,000 \text{ cm}^2 \text{ V}^{-1} \text{ s}^{-1}$ with the carrier density of $2.0 \times 10^{11} \text{ cm}^{-2}$ at 0.04 K, estimated from low-field Hall effect. This mobility corresponds to the transport scattering time of $\approx 50 \text{ ps}$, which is approaching the supreme value of the extremely clean 2DEG in AlGaAs/GaAs.

For the MgZnO/ZnO sample, we measured magnetotransport properties in a dilution refrigerator, where the sample was placed in a perpendicular magnetic field created by a cryogen-free hybrid magnet with the maximum magnetic field of 27.5 T. Fig. 1 shows the result of the measurement at 0.04 K. Longitudinal resistance (R_{xx}) shows clear Shubnikov-de Haas oscillations starting at a low magnetic field of 0.3 T, which suggests high quality of the sample. As in the previous report [2], we observed the fractional states at $\nu = 5/3$ and $4/3$. Additionally, a number of fractional states $\nu = 2/3$, $3/5$, and $2/5$ in the lowest Landau level are observed. The most remarkable observation is the appearance of the fundamental fractional state $\nu = 1/3$ at $B = 25.5 \text{ T}$ [3].

The observation of the $\nu = 1/3$ state in the oxide heterostructure opened a new door to utilize more degrees of freedom in mesoscopic systems. In particular, oxide materials have much variety of crystal structures because of their ionic character, which is strongly correlated with electronic band structure and spin-orbit interaction. For example, in wurtzite structure as in ZnO, linear k dependence in the valence band is predicted, which is expected to exhibit a strong relativistic effect. Realizing mesoscopic systems using such new material systems will create a new field in condensed matter physics.

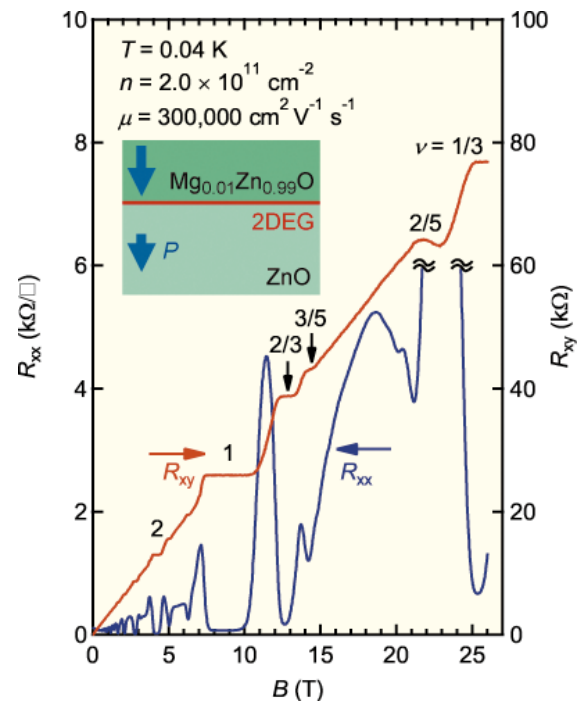


Fig. 1: Magnetotransport properties of two-dimensional electron gas at a MgZnO/ZnO heterointerface at 0.04 K. The inset shows the schematic diagram of the heterostructure.

References

- [1] A. Tsukazaki, A. Ohtomo, T. Kita, Y. Ohno, H. Ohno, and M. Kawasaki, *Science* **315**, 1388 (2007).
- [2] A. Tsukazaki, S. Akasaka, K. Nakahara, Y. Ohno, H. Ohno, D. Maryenko, A. Ohtomo, and M. Kawasaki, *Nature Mater.* **9**, 889 (2010).
- [3] Y. Kozuka, A. Tsukazaki, D. Maryenko, J. Falson, S. Akasaka, K. Nakahara, S. Nakamura, S. Awaji, K. Ueno, and M. Kawasaki, *Phys. Rev. B* **84**, 033304 (2011).

Keywords: oxide, electrical property
 Y. Kozuka¹, A. Tsukazaki^{1,2}, D. Maryenko³, J. Falson⁴, S. Nakamura⁴, S. Awaji⁴, K. Ueno^{2,5}, and M. Kawasaki^{1,3,6,7}

1)Graduate School of Engineering, QPEC, The University of Tokyo, 2)JST-PRESTO, 3)Correlated Electron Research Group, RIKEN-ASI, 4)IMR, Tohoku University, 5)Graduate School of Arts and Sciences, Department of Basic Science, The University of Tokyo, 6)WPI-AIMR, Tohoku University, 7)JST-CREST

E-mail:kozuka@ap.t.u-tokyo.ac.jp

Plastic Working of Metallic Glass Bolts by Cold Thread Rolling

A Zr-based metallic glass (MG) bolt with a single glassy phase was successfully produced by cold thread rolling. Large plastic strain without destructive crack propagation is induced at the screw thread near the surface of the cylindrical specimen due to the compressive mean stress distributions developed throughout the thread rolling process. The process design based on this mechanism can significantly contribute to MG applications.

Bolts are commonly employed machine elements used for joining and fastening, and their performance and reliability influence the overall performance of machines. In this study, we have plastically worked and formed bolts using metallic glass (MG) that exhibits unique mechanical properties such as high tensile strength, low Young's modulus, and large elastic limit. The large elastic limit increases the permissible elongation range of the bolt and helps avoid bolt loosening, while the low Young's modulus effectively resists screwed-in bolt loosening by increasing the frictional forces on both bolt-nut contact area and bearing surface. We employed a zirconium-based MG $Zr_{55}Al_{10}Cu_{30}Ni_5$ for our experimental investigations. A pre-form of a hexagon socket head cap screw (bolt) was fabricated by squeeze casting. Cold and warm thread rolling were performed to form a metric screw thread M3x0.5 (class 6g (ISO)) below the glass transition temperature using a flat rolling machine as shown in Fig.1. Despite the extremely poor ductility of MG at room temperature[1], thread rolling was successfully performed[2].

From experimental investigations and straining analysis by the three-dimensional finite element method (3D-FEM), we found that the mechanisms of the plastic deformation are as follows:

(1) Straining occurred over a limited area near the surface of the cylindrical specimen due to the stress distributions during thread rolling.

(2) Large plastic strain without destructive crack propagation is induced at the screw thread due to the compressive mean stress distributions developed throughout the thread rolling process.

(3) Fundamentally, thread rolling is an incremental formation process. The effects of preliminarily introduced strain work favorably by increasing the MG ductility in the deformed region.

The tensile strength of the thread-rolled bolt was approximately 1600 MPa, which is considerably higher than that of conventional heat-treated high strength steel bolts. We believe that the process design based on these mechanisms of plastic working of MG can significantly contribute to MG applications.

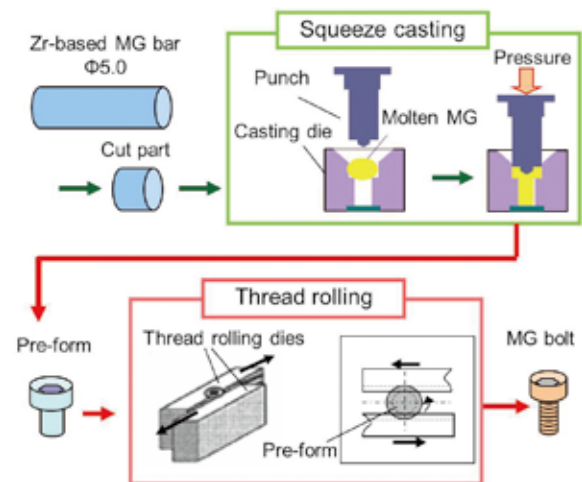


Fig.1 Processing procedure for Zr-based metallic glass (MG) bolt

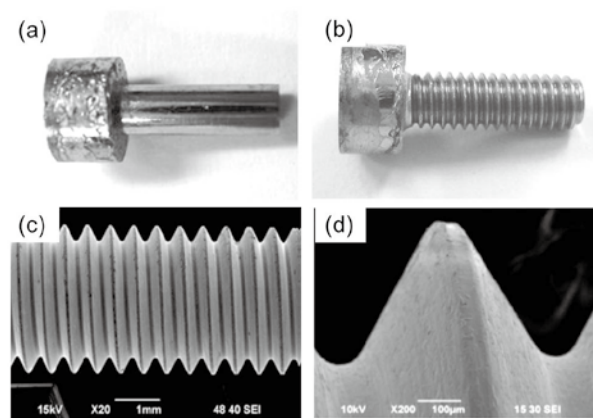


Fig.2 (a) Pre-form for metallic glass (MG) bolt processed by squeeze casting; (b) thread-rolled MG bolt at RT (293 K); (c) SEM microphotograph of screw thread; (d) magnified image of ridge, groove, and flank of the screw thread (c)

References

- [1] H. Kato, H. Igarashi and A. Inoue, *Mater. Lett.* 62, 1592 (2008)
- [2] S. Yamanaka, K. Amiya, Y. Saotome and A. Inoue, *Mater. Trans.*, 52, 243(2011)

Keywords: metallic glass, plastic working
Y.Saotome¹, K.Amiya¹ and S. Yamanaka²

1) Osaka Center for Industrial Materials research

2) Maruemu Works Co. Ltd.

E-mail:saotome@imr.tohoku.ac.jp

URL:http://www.kansaicenter.imr.tohoku.ac.jp

Osaka Center for Industrial Material Research.

Collaboration project (Osaka Center) between IMR, Osaka Prefecture Government and enterprises in Osaka area (especially for Higashi Osaka) sponsored by Ministry of Education, Culture, Sports, Science and Technology has been completed on March 2011. Through five years activities such as responding to inquiries from industries and solving them, introducing academic research outputs to transfer to industries, and educate material science regarding application to researchers and technicians in industries in order to enhance their core manufacturing technology, Osaka Center has established the status in Kansai area to promote academia-industry-government cooperation.

Osaka Center was established in Osaka as a special division in the Institute for Materials Research, Tohoku University in April 2006 based on an agreement with Osaka Prefecture Government. This is the first collaboration project in Japan between national university and local government sponsored by government (Ministry of Education, Culture, Sports, Science and Technology). It consists of laboratories dedicated to research and development of nano-structured metallic materials with the application viewpoints based on the materials science, and they are associated with research organizations in Kansai area. There are 6 groups in Center; Preparation, Fabrication, and Processing of New Materials, Applied Science of Microstructural Controlling, Bio-Materials, and Administrative Office. The scope of project is to understand the fundamentals of metallic materials and rapid realization of their application to industry, especially, small and medium enterprises in Osaka area. The second mission is to solve technical problems in the enterprises under collaboration with Development Center for New Metallic Material in Osaka Prefecture University. And the third is to educate material science related to industrial application to next generation materials scientists and researchers in universities and enterprises.

Throughout five years' activities, Osaka Center produced several distinguished achievements. First, six professors in Osaka Center responded technical inquiries from industries by themselves, where the system is different from that of other universities (usually, coordinators employed by university hear the inquiries and conveyed suitable professors to respond the inquiries). Figure 1 shows the number of inquiries from industries at Creation Core Higashi Osaka (governmental body, where sixteen local universities and one college are located to respond inquiries from industries). A smooth increase of the inquiries with year is evident: 102 in 2007, 263 in 2008, 307 in 2009 and 400 in 2010. The location of the company's head office is shown in the left figure of Fig. 2,

and the inquiries are categorized as shown in the right figure of Fig. 2. This suggests that Osaka Center has been recognized in whole Kansai area including Osaka prefecture, and expected to be a technical advisor in the manufacturing industry.

Secondly, Osaka Center has opened technical seminars on special topics twenty-four times to provide scientific knowledge to technicians and researchers in industries. The

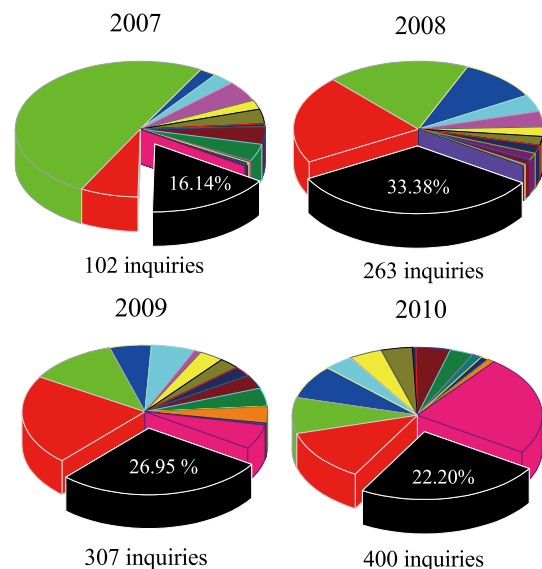


Fig.1 Fraction of inquiries from industries at Creation Core Higashi Osaka (Sixteen local universities and one college are located): the black part of circle chart corresponds to Osaka Center.

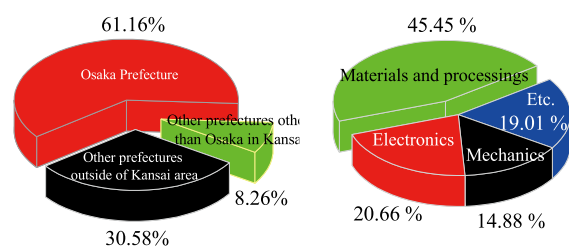






Fig. 2 Analysis of inquiries from companies to Osaka Center; the location of company (left) and category of inquired content (right).

seminars were organized by the professors in Center and the topic was selected based on the industrial needs. Some of the seminars were held under collaboration with scientific societies. Further, the Center professors have lectures on materials design, technical skills and related fundamentals of materials science to the students in Osaka Prefecture University for the purpose of demonstrating the importance of material science contributing to industrial applications. Thirdly, Osaka Center participates in various technical exhibitions or seminars organized by local governments, publishers, financiers and incorporated foundations upon request to introduce the academic research outputs to industries and transfer them to applications. Through these activities, twenty-seven collaboration research

projects between the Osaka Center and companies have been established and thirty innovations were applied for patents. Some of the collaboration studies have obtained competitive research funds from governments. As an example, Table I summarizes the output of production research project sponsored by Osaka Prefecture in 2007. This project is carried out by collaboration between Osaka Center and enterprise in Osaka Prefecture.

Following the Osaka Center project, IMR has extended the activities of Osaka Center to the whole Kansai area under collaboration with Osaka Prefecture Government, which was adopted by Ministry of Education, Culture, Sports, Science and Technology. This new project started in April 2011, and Kansai Center was launched to replace Osaka Center.

Table 1 Summary of collaborative research project sponsored by Osaka Prefecture

(a) Title (b) Academic members	Summary	
(a) Development of water purification device by using TiO ₂ photocatalysts. (b) Tohoku University Prof. Naoya MASAHASHI Assist. Prof. Yoshiteru MIZUKOSHI	Anodic TiO ₂ photocatalysts immobilized on the surface of lath-structured Ti effectively bleached methylene blue aqueous solution and exhibits superhydrophilicity. This device is expected to purify contaminated water.	 TiO ₂ coated lath Ti incorporated in water purification equipment
(a) Development of surface-hardened Ni base dual two-phase intermetallic alloys (b) Osaka Prefecture University Prof. Takayuki TAKASUGI Assoc. Prof. Yasuyuki KANENO	Optimal plasma-carburizing and -nitriding condition of Ni base dual two-phase intermetallic alloy was found. Also, the alloy compositions suitable for plasma surface hardening were developed.	 Plasma-carburized Ni base dual two-phase intermetallic alloy used for FSW tool
(a) Size control of nickel oxide nanoparticles (b) Tohoku University Prof. Toyohiko KONNO	Ni oxide nanoparticles with an average diameter of 90 nm are now constantly fabricated, and dispersed in a liquid phase without agglomeration by taking an advantage of surfactant technology.	 Transmission Electron Microscopy image of Ni oxide particles
(a) Development of the diffractive optical components of metallic glass (b) Tohoku University Prof. Yasunori SAOTOME Assoc. Prof. Hisamichi KIMURA	Nano-imprinting technique of the metallic glass was successfully applied to the fabrication of diffraction gratings with a period of nano-order.	 Surface morphology on nano-imprinted metallic glass

Keywords: partnership between industry, academia and government, technology transfer
N.Masahashi (Kansai Center for Industrial Materials Research)
E-mail: masahasi@imr.tohoku.ac.jp
URL: <http://www.kansaicenter.imr.tohoku.ac.jp>

Magic Monatomic Mn Nanowire Self-Assembly on Si(001)

We show here by *ab initio* calculations that an atomistic nucleation process of monoatomic Mn nanowire self-assembly on Si(001) to form a new magic $3n+1$ atom dense trimerlike linear chains (DTLCs) driven by pedestal site adsorption. Moreover, the length of DTLCs is limited by a competing process to form three-dimensional D_{3h} -Mn₅ clusters in early stages.

There has been considerable interest in recent years in manganese and manganese silicide as promising candidates for spintronics applications. STM studies reveal that room temperature deposition leads to preferential formation of monoatomic Mn wires in early stages, and small clusters appear at higher coverage and compete with the wire growth. Understanding the precise nature of Mn adsorption sites, the bonding to the Si surface and the growth mechanism of the nanowire structures is critical to predicting and tailoring Mn-Si nanostructure properties.

We here first explore possible diffusion pathways for a single Mn adatom on Si(001). When a Mn atom adsorbs on the stable pedestal site P, three possible diffusion pathways P1, P2, and P3 are considered [1]. The relative energies are plotted in Fig. 1. The energy barriers are estimated to be 0.49, 0.48, and 1.06 eV for P1, P2, and P3, respectively. These results clearly show that Mn adatoms can easily diffuse along or across the dimer rows, but are kinetically limited for diving into the subsurface layer or diffuse into the deep layer at room temperature on Si(100). To understand the competing nature in the formation of the DTLC and 3D clusters, finite dense trimerlike linear chains starting from an isolated Mn on the pedestal site are examined. In Fig. 2, we plot the binding energy versus the pathways to form the dense-monoatomic Mn wires and D_{3h} -Mn₅ cluster on Si(001). We find that Mn adatoms on Si(001) prefer forming a finite DTLC with magic number of $3n+1$ (4, 7, 10, ...), perpendicular to the surface dimer rows. They always start from and end on the P site, driven by the favorable pedestal site adsorption shown above. These $(3n+1)$ magic DTLCs are more stable than the PM dimer with a large dissociation barrier (1.12-1.28 eV for $n = 1, 2$), and their binding energies become lower monotonically as n increases. Because of the induced strain along the wire stretching direction, the Mn on P site is pushed down into the substrate, and two M site Mn adatoms over the trough show a buckled dimerlike configuration with stress relief (see Fig. 2). Meanwhile, D_{3h} -Mn₅ cluster exhibits similar energetic stability, showing the competing growth nature between the wire and 3D cluster.

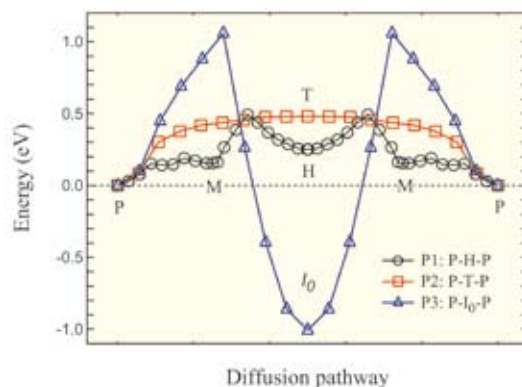


Fig.1 Relative total energy versus the reaction pathways for ad-Mn diffusion on Si(001) surface. P1: P->H->P is a hopping pathway, across the dimer rows; P2: P->T->P is a rolling-over pathway, parallel to the dimer rows; P3: P->I₀->P is an insert pathway along the surface dimer row.

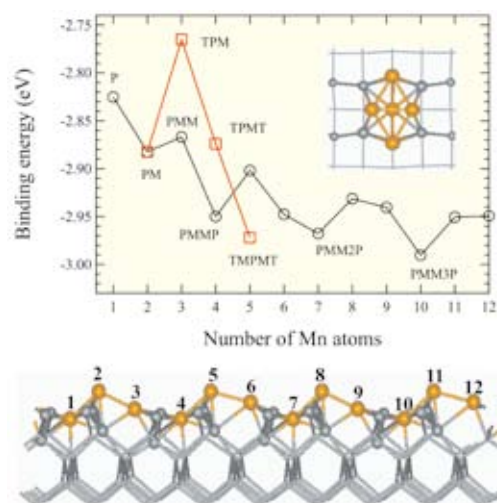


Fig.2 Atomic binding energy versus the pathways to form a monoatomic Mn-wire (o) or cluster (□) on Si(001).

References

- [1] J.T. Wang, C.F. Chen, E.G. Wang, and Y. Kawazoe, Phys. Rev. Lett. 105, 116102 (2010).

Keywords: nanowire, 3d-metal, silicon surface
 J.T. Wang¹, C.F. Chen², E.G. Wang¹, Y. Kawazoe³
 1) Institute of Physics, CAS, 2) Department of Physics, UNLV, 3) IMR, Tohoku University
 E-mail: wjt@aphy.iphy.ac.cn
<http://js.caseeducation.cn/JS/~wjt>

Detection of Rare Earth Dopants at the Atomic Level in YAG-based Optical Ceramics

In complex oxides, metallic and oxygen atoms occupy several crystallographically non-equivalent sites. The electronic states of the impurities are thus expected to have their origin not only in the nature of impurity atoms themselves, but also in the symmetry of the substituted sites. By employing wave-front reconstruction techniques on high-resolution TEM images taken under Cs-corrected conditions and Z-contrasts in atomically resolved STEM, we can directly clarify the favorable sites for dopant atoms.

Understanding the optical properties of materials requires a detailed investigation of their microstructure, especially regarding the exact location of the required dopants (e.g. rare earth elements such as Ce^{3+} , Nd^{3+} or Yb^{3+}). For example, it was recently shown by careful Transmission Electron Microscopy (TEM) observations that Ce strongly segregates at grain-boundaries within YAG (Yttrium Aluminium Garnet $Y_3Al_5O_{12}$) [1].

STEM-HAADF imaging (Scanning TEM in High Angle Annular Dark Field) consists in scanning the electron probe on the sample, and collecting on an annular detector the primary electrons scattered at high angle. In such a process, the scattered signal is roughly proportional to Z^2 , where Z is the atomic number of the probed species. Then, heavy atoms (such as rare-earth elements) give rise to a brighter contrast than lighter species (such as O, Al and even Y in the YAG structure). Atomic resolution is achieved if the probe size is smaller than the interatomic distance within the material of interest under some specific viewing crystallographic directions.

We have performed both High Resolution (HR) and HAADF imaging on pure YAG and Yb-doped YAG polycrystals, using a TITAN FEI electron microscope, operating at 300 kV. On the one hand, this instrument is equipped with a Cs aberration corrector on the objective lens, allowing a resolution down to 0.1 nm to be obtained in the HREM mode [2]. On the other hand, it is also equipped with an annular detector collecting electrons in a 70-210 mRad angular range. Nanoprobe chemical analysis was also simultaneously performed using an EDAX EDX (Energy-Dispersive X-ray) analyser mounted on the microscope.

Whereas Cs-corrected HREM failed to reveal the distribution of Yb-containing atomic columns, the STEM-HAADF imaging mode appeared to be more efficient owing to its sensitivity to Z. Fig. 1 shows a comparison of a 1.4 at.% Yb-doped and a pure YAG samples when observed along the [001] azimuth. A high density of brighter columns is observed for the doped material, which can be consistently

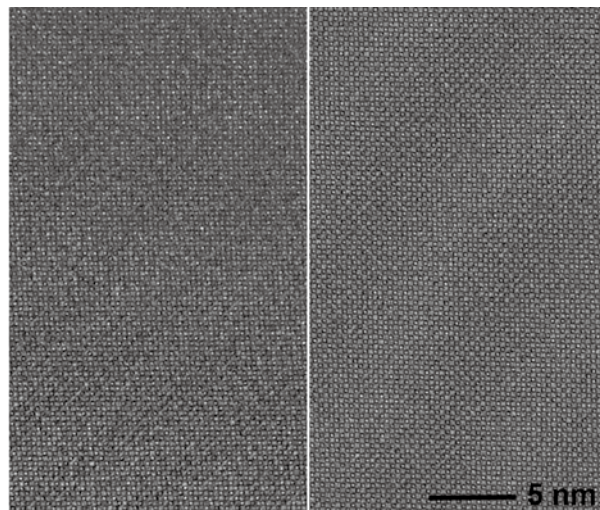


Fig. 1 HAADF-STEM images of two regions of similar thicknesses (as attested by low-loss EELS spectra) from a 1.4 at. % Yb-doped sample (left) and a pure YAG sample (right).

analysed in terms of statistics as imaging Yb-containing atomic columns. Dedicated HAADF-STEM image simulations confirm this finding. This work shows that no segregation, neither clustering of Yb ions occurs in polycrystalline YAG.

References

- [1] W. Zhao, C. Mancini, D. Amans, G. Boulon, T. Epicier, Y. Min, H. Yagi, T. Yanagitani, T. Yanagida, A. Yoshikawa *Jpn. J. Appl. Physics* 49 (2010) 022602
- [2] K Sato, T.J. Konno, Y. Hirotsu, , *J. Appl. Phys.* **107** (2010) 024304.

Keywords: optical ceramics, Yb-doped YAG, atomic STEM-HAADF
 T. Epicier (INSA-Lyon) and T.J. Konno
 E-mail: thierry.epicier@insa-lyon.fr, tjkonno@imr.tohoku.ac.jp
 URL: <http://clym.insa-lyon.fr>, <http://konno-lab.imr.tohoku.ac.jp/>